Scottish Universities Environmental Research Centre

Comments on Quaternary landscape evolution in the vicinity of the Souskiou-Laona excavation, Cyprus

May 2012

T.C. Kinnaird[1] and J.E. Dixon[2]

[1]SUERC, East Kilbride, G75 OQF
[2]170 Newbattle Abbey Crescent, Eskbank, Dalkeith, EH22 3LS

East Kilbride Glasgow G75 0QF Telephone: 01355 223332 Fax: 01355 229898

University of Glasgow
The University of Glasgow, charity number SC004401

The University of Edinburgh is a charitable body, registered in Scotland, with registration number SC005336

Comments on Quaternary landscape evolution at the *Souskiou-Laona* excavation, Cyprus, May 12th - 18th 2011

Tim C. Kinnaird and John E. Dixon

1. Introduction

Geological investigations and geomorphological mapping were undertaken in the region around Sousikou-Laona by John Dixon (May 2010) and Tim Kinnaird (May 2011).

2. Objectives

1. To establish a relative chronology for the landforms in the vicinity of Sousikou-Laona, through the identification and correlation of the various erosion surfaces and channel fills, and if possible correlation with the Paphos marine terraces and fanglomerate sequence.
2. To determine the incision history of the Vathyrkakas ravine, and the formation of the associated Laona ridge.
3. To investigate the relationship between the settlements on the Laona ridge, with the local geomorphology, to determine the evolution of the slopes during and since the period of occupation.

3. Geomorphological setting

The Sousikou complex of settlement and cemeteries is located on an elevated spur, trending NE-SW, at the confluence of the Dhiarizos and Aragin Vathin rivers; its northwestern slopes were cut by the Dhiarizos river, and the southeastern slopes by the Aragin Vathin river (the Vathyrkakas ravine; **Fig. 1**). The spur itself is designated by the toponym *Laona*. Both the northwestern and southeastern slopes of the ridge are steep with precipitous falls of ~ 100 m to the Dhiarizos and Aragin Vathin riverbeds. Both slopes are active, with erosional gullies, landslides and significant colluvial deposits.

The Vathyrkakas ravine separates the Laona ridge from the Vathyrkakas plateau to the east. The ravine is incised into bedrock consisting of bedded tabular calcarenites and softer marls (of the Miocene Pakhna Formation, see section Geological setting), and gravel terrace deposits of probable Early Pleistocene age (**Fig. 2**). A hard capping of kafkalla limestone is preserved locally along both the Laona ridge and Vathyrkakas plateau. The shaft graves on the top of the ridge, and on the Vathyrkakas plateau, are cut into degraded Pakhna chalks and marls.

In its lower reaches, the Vathyrkakas ravine is a narrow channel, incised into Pakhna Formation chalk and marl (**Fig. 3**). The base of the Vathyrkakas ravine appears to hang 2 m above the level of the Dhiarzos river bed (**Fig. 4**). The actual exit channel of the ravine is obscured by vegetation. To the southwest of the channel exit, there is a 6 m high cliff of Pakhna Formation chalk, which is capped by c. 1 m of colluvium (**Fig. 4**). A prominent large field occurs at the height of the 6 m high cliff. It is possible that this 6 m+ surface is a relict terrace, albeit modified, and the ravine has cut down later to 2m+. The most recent incision of the Dhiarzos has removed the entire 2m+ terrace opposite the field and cut into the bedrock, but has not cut into the small 2m+ ravine exit.

Figure 1: Satellite image (Google Earth) of the region around the *Souskiou-Laona* excavation. The *Laona* ridge is marked by the black arrow. The incised feature to the right of the arrow is the *Vathyrkakas* ravine, which seasonally, contains the ephemeral *Aragin Vathin* river. The plateau to the right of the ravine is designated by the toponym *Vathyrkakas.* The main river valley (to the left of the arrow) contains the *Dhiarzos* river.

Figure 2: Photograph of the *Sousikou-Laona* ridge. The photograph is taken from a vantage point on the east-facing slope of the *Vathyrkakas* ravine.

Figure 3: View of the *Vathyrkakas* ravine, looking east across the *Dhiarzos* river, from the village of Nikokleia. A close up of the area delineated by the red box is shown in figure 4.

Figure 4: Photograph of the entrance to the *Vathyrkakas* ravine. The base of the *Vathyrkakas* ravine hangs 2 metres above the level of the *Dhiarzos* river bed. To the southwest of the channel exit, there is a 6 m high cliff of Pakhna Formation chalk, which is capped by c. 1 m of colluvium. A prominent large field occurs at the height of the 6 m high cliff.

4. Geological setting

The underlying geology to the Laona ridge consists of bedded tabular chalks, calcarenites and marls of the Miocene Pakhna Formation. The ridge itself is capped by a gravel terrace of probable Early Pleistocene age; the gravels overlie a very degraded Pakhna Formation chalk/marl surface, which is a regional erosional surface.

Bedrock geology

The bedrock geology to the Souskiou-Laona ridge is the Miocene Pakhna Formation (c. 20-5 Ma; Eaton and Robertson, 1993). To the north of the study area, in the area of the topographically elevated Oreites Forest block (on which the Oreites Windfarm is built), the bedrock geology is the Paleocene - Oligocene Lefkara Formation (c. 60 - 20 Ma; Kähler and Stow, 1998). The Lefkara Formation occupies a lower stratigraphic position than the Pakhna Formation.

In the vicinity of the Souskiou-Laona settlement and cemeteries, the bedrock geology consists of tabular, competent beds of chalk and calcarenite, 10 - 40 cm thick, interbedded with less competent beds of marl and reworked chalk, 10 of centimetres thick. Bedding in the Pakhna succession dips at a shallow angle to the south/southwest. (The beds of marl and reworked chalk are less resistant to erosion than the beds of chalk and calcarenite; this has led to the 'stepped profile' on the slopes to the Vathyrkakas ravine.)

The bedrock geology, in the vicinity of the ridge, is cut by a number of faults and fractures which trend N-S to NNW-SSE (**Fig. 5**; Appendix B: Fault trends in the bedrock geology). The faults occur at a variety of scales, with offsets ranging from tens of centimetres (micro-scale faults; **Fig. 5**) to tens of metres (meso-scale faults; **Fig. 6**). The majority of the faults displace strata in a normal sense, based on offset strata and the orientation of drag folds (**Figs 5 and 6**); where present, slickenlines on slickensided fault planes, indicate that this displacement is dip-slip to slightly oblique slip. The faults are old features, with their origins in geological time, specifically the Late Miocene; the faults formed in response to E-W-directed extension, related to the roll-back of the subduction zone to the south of Cyprus, and extension in the overlying plate (Kinnaird and Robertson, 2012). A number of the faults appear to have been re-activated in a strike-slip sense; the N-S striking faults in a left-lateral sense, and the NNW-SSE striking set in a right-lateral sense. At one, possibly two localities, it is possible to trace the re-activated faults into late Pleistocene deposits that are locally deformed.

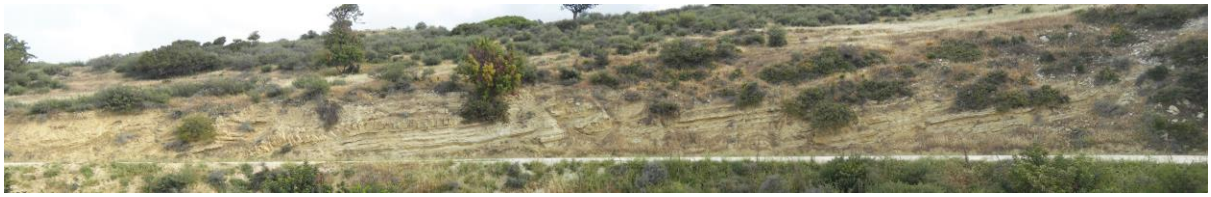

Figure 5: Structural trends in the bedrock geology. Outcrop of Pakhna Formation chalk at the point where the Kouklia-Souskiou dirt road crosses the Vathyrkakas ravine.

Figure 6: Photograph of the Sousikou-Laona excavation (marked by black arrow), looking south along the valley axis of the Vathyrkakas ravine, from a vantage point northwest of the excavation; the photograph illustrates the steep precipitous slopes of the Laona ridge and Vathyrkakas plateau, note the stepped profile of the slopes formed in response to differential weathering of competent calcarenite horizons and less resistant marl horizons. The bedrock geology is cut by a number of N-S to NNW-SSE trending faults and conjugate NNW-SSE and E-W fractures (one such fault is marked by the red arrow).

The re-activation of the Late Miocene faults occurred in the late Pliocene – early Pleistocene, when the Eratosthenes Seamount collided with the Cyprus trench, resulted in a switch to an E-W transpressional tectonic regime (Kinnaird and Robertson, 2012)

The faults all formed in geological time; however it is important to note that the faults delineate zones of weaknesses along which slope failures may have occurred during the Chalcolithic to the present day.

Superficial geology

The Laona ridge is capped by gravels of probable Early Pleistocene age; the gravels overlie a degraded bedrock surface, which is believed to be a regional erosional surface. Is it possible to correlate this geomophological feature, and the other landforms in the vicinity of Sousikou-Laona,

with the Fanglomerate sequence and Paphos marine terraces, so that these features can be placed in a relative chronology?

Poole and Robertson (1991) identified a number of regional erosional surfaces in southwest Cyprus, which they designated F0 (oldest) to F4 (youngest); the younger units occur at progressively lower topographic levels. These erosional surfaces are in places, overlain by coarse conglomerates and other sediments, including caliche and palaeosols (the Fanglomerate Group; Poole and Robertson (1991)). These sediments are subdivided into four informal units, termed F0 to F4, after the erosion surface they overlie, or the erosion event they formed in response to.

Table 1 lists the various regional erosional surfaces and associated deposits that have been identified in the vicinity of the Sousikou-Laona settlement and cemeteries. The oldest known erosion feature in the vicinity of the Sousikou-Laona ridge, is a mature erosion surface of Late Pliocene - Early Pleistocene age, at approximately 260 m above present mean sea level, preserved at a road cut on the Kouklia-Archimandrita road (**Figs 7 and 8**). 5 m of coarse immature, poorly sorted, clast- to matrix-supported conglomerates, with subordinate amounts of finer-grained clastic sediments, directly overlie degraded Pakhna Formation chalk; the gravels are in turn overlain by red terra rossa– type palaeosols and caliche horizons. A second distinct terrace is developed at ~ 100-180 m above mean sea level, this erosion surface forms the Vathyrkakas plateau, and the flat ground on top of the Laona ridge. The photograph of the Vathyrkakas plateau, taken from a vantage position on the Kouklia-Archimandrita road, illustrates the planar nature of this erosion surface (**Fig. 9**). In the nomenclature of Poole and Robertson (1991; 1998) the terraces would be termed F0 and F1, respectively. If the erosion surface forming the Vathyrkakas plateau is traced south towards Kouklia, the surface passes into an aggradation surface (the F1 cliffline?), on which (just outside Kouklia) there is an accumulation of 4 m of matrix-supported boulder and pebble conglomerates. Here, massive, structureless, grain- to matrix-supported coarse conglomerates are overlain by more mature, generally well-bedded and well sorted conglomerates, sands and silts. These deposits are correlated with the F2 Fanglomerate unit.

The Vathyrkakas plateau was incised by the proto-Aragin Vathin river in F2 or younger times, as the ravine intersects the regional F1 surface. In the lower reaches of the ravine (defined here, as the area southwest of *Souskiou-Chapel*) a number of terrace deposits, or channel fills, are preserved as isolated outcrops on the flanks of the ravine. The height at which these deposits are preserved relative to the ravine bottom place them in a relative chronology: the oldest deposits have been left hanging several metres above the present base of the ravine, these deposits are comprised of clast- and matrix-supported cobble and pebble conglomerates, comprised of sub-rounded to rounded clasts of dolerite, and angular blocks of chalk and calcarenite (Early Fill; **Fig. 10**); younger deposits are preserved as isolated outcrops within the valley axis, as matrix-supported pebble conglomerates, with sub-angular to sub-rounded clasts of chalk, limestone and calcarenite (Late Fill; **Fig. 10**). Interestingly, the average clast size within the 'older' deposits (up to 60 cm in diameter) is significantly larger than those in the 'younger' deposits (less than 30 cm in diameter), suggesting that the flows became significantly less intense during the late Pleistocene and Holocene. The youngest accumulation of fluvial sediment in the ravine is preserved as the back-fill to a ruined 18th/19th century mill (E. Peltenburg, personal communication), located downstream of where the Sousikou-Laona access road intersects with the ravine. This 'recent' channel fill is cut directly into an older terrace deposit, a boulder-conglomerate, comprised of large rounded to sub-rounded boulders of calcarenite (> 70 cm in diameter), which are chaotically organised, and attest to a period when water was abundant in the channel. The 'recent' accumulation is confined to a channelized unit 1.5 m deep and 5-6 m wide: the

base is marked by matrix-supported cobble- and pebble conglomerates, which are moderately stratified, and contain imbricated, poorly sorted, sub-rounded immature clasts of abundant chalk, calcarenite, limestone (mm to cm in diameter) and subordinate diorite (mm in diameter); the conglomerates then grade into brown-clay rich soil, which contains burrows and rootlets. The lack of stratigraphic and topographic constraints within the ravine prevents the correlation of these deposits with the chronological framework of Poole and Robertson (1991; 1998)

In the wider region, a F2 age or younger channel fill, is preserved 'hanging' in the cliffs that abut the *Kouklia-Dhiarzos* access road (cut obliquely by the present scarp). The 'F2' palaeo-channel is incised into both bedded Pakhna Formation chalk, i.e. on its western flank, and older colluvial/gravel deposits, i.e. on its eastern flank. The 'F2' channel has exploited natural weaknesses in the bedrock geology, such that the western margin of the channel is aligned parallel to fractures in the bedrock, and is juxtaposed against one such fracture plane. The eastern margin of the channel is poorly exposed owing to recent slope collapse and vegetation. The clast assemblage within this channel fill is dominated by igneous rocks derived from the Troodos Massif, and to a lesser extent calcarenites and chalks from the local bedrock. Mamonia- type sediments are absent (**Fig. 10**).

The youngest erosional feature in the vicinity of the Sousikou-Laona ridge is the Dhiarzos river valley. In the chronological framework of Poole and Robertson (1998), it would be stated that the present-day Dhiarzos river is incised to near the F4 level. The valley floor is covered by sands and silts, and massive, poorly sorted immature conglomerates. The conglomerates range from clast-supported units in channels, to matrix-supported units, interbedded with the fine sands and silts, in the overbank units. Clasts are locally imbricated, poorly sorted, immature, angular to rounded, and are dominated by lithologies derived from the Mamonia Complex (i.e. limestones and sandstones) and local bedrock (i.e. calcarenites and chalks). Coarse-grained igneous rocks are subordinate (**Fig. 10**). Remnants of the F3 Fanglomerate unit are preserved in isolated and sparse outcrops along the length of the Dhiarzos river, up to 15 m above the present-day channel.

Position	Location	Description	Elevation (a.m.s.l)	Inferred age
N34°43.412' E032°36.415'	Roadcut on the Kouklia-Archimandrita	Marine Terrace (F0)	260m	Late Pliocene
N34°43.536' E032°36.424'	Sousikou-Laona ridge	Fanglomerate (F1)	180m	Latest Pliocene/Early Pleistocene
N34°42.678' E032°24.762'	Kouklia	Fanglomerate (F1 cliff line?)	85 m	Latest Pliocene/Early Pleistocene
N34°43.464' E032°34.789'	Vathyrkakas Ravine	Fanglomerate (F2 or F3?)		Mid to Late Pleistocene
N34°43.464' E032°34.789'	Mouth of Vathyrkakas Ravine	6m+ Fluvial Terrace	60m	Mid to Late Pleistocene; earlier than the 2m+ terrace
		2m+ Fluvial Terrace	54m	Early Pleistocene; later than the 2m+ terrace
N34°43.468' E032°34.753'	Dhiarzos riverbed	Fluvial Terrace (F4)	~50m	Modified in the Recent

Table 1: Prominent erosional surfaces, with associated sediments, in the vicinity of the Sousikou-*Laona* excavation

Figure 7: Photograph of the highest marine terrace in the Sousikou region. The terrace occurs at an elevation of 258 m a.m.s.l;

Figure 8: Bivalve burrows on a large boulder at the base of the 258 m terrace; evidence the terrace was deposited in a marine setting

Figure 9: Photograph of the Vathyrkakas ravine, taken from a vantage point on the Kouklia-Archimandrita road

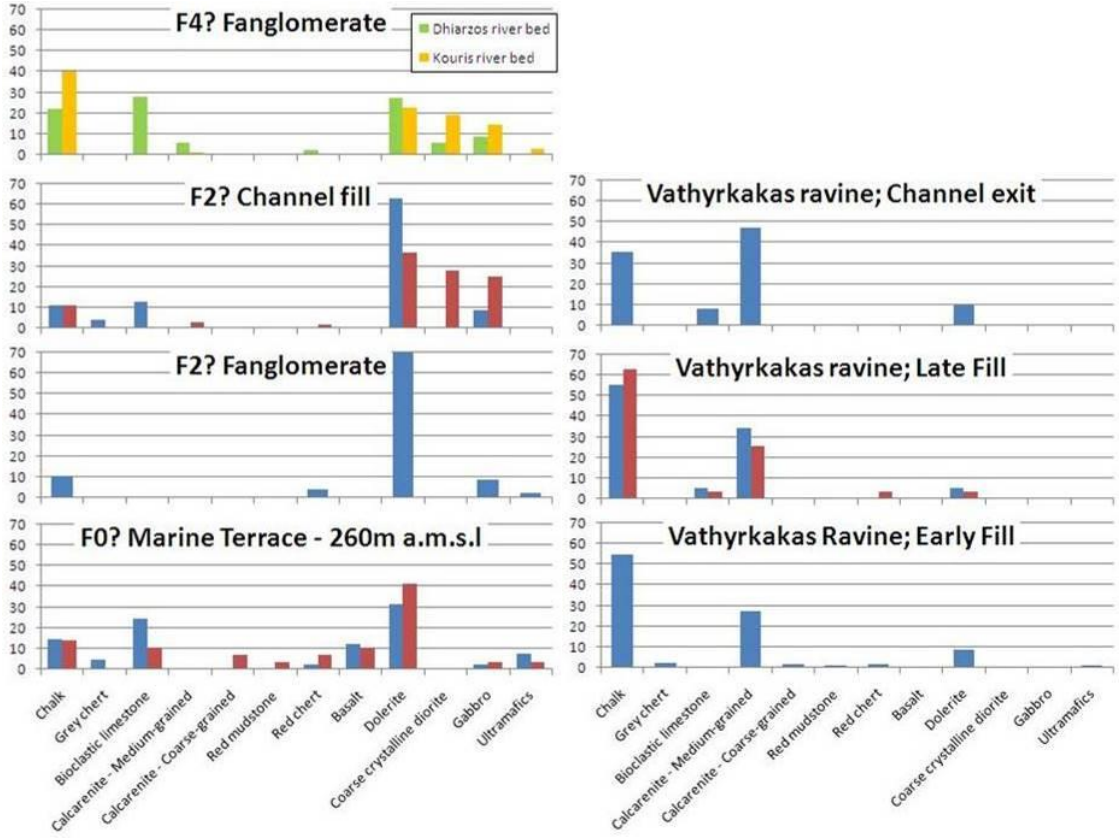

Figure 10: Provenance data from prominent geomorphological features (and the associated sediments) in the Sousikou-*Laona* region; where possible, the units have been correlated with the existing stratigraphic framework of Poole and Robertson (1991; 1998, 2000). Clasts of erosionally resistant lithologies, notably ophiolitic diabase and Miocene reef-related limestone, are volumetrically over-represented, relative to friable basalt and early Tertiary pelagic carbonate sediments.

5. Landscape evolution

Late Pliocene – Quaternary landscape evolution in the vicinity of Sousikou

The Troodos Massif experienced strong focused uplift in the late Pliocene to late Pleistocene (Kinnaird et al., 2011; Poole and Robertson, 1991; 1998) with less intense uplift continuing into the Quaternary (Poole et al., 1990). This uplift created considerable topographic relief, and with the wetter climate in this interval, caused large quantities of Troodos material to be eroded and transported away from the centre in major rivers. As uplift was focused on the 'centre' of the island, this resulted in a radial pattern in the distribution of coarse fluvial facies (Fanglomerates), away from the massif (Poole and Robertson, 1991; 1998). At times of relative sea-level (RSL) high during the late Pliocene - late Pleistocene interval, terrestrial terraces developed inland by fluvial processes, associated with sediment aggradation. Whereas, at the coast, in areas starved of clastic sediment input (e.g. SW and SE Cyprus), low-lying, marine terraces were cut, and overlain by littoral bioclastic calcarenites.

The continuing uplift of the Troodos Massif and periodic falls in global sea-level through the late Pliocene to late Pleistocene interval caused the fanglomerates to be progressively uplifted relative to sea-level and incised, as the rivers cut down to successive new base-levels. The effect of this is that

the oldest fanglomerate surfaces are now left stranded on the tops of low hills, as in the area around the Sousikou site. The very highest point on the ridge into which the burial chambers are cut is a patch of the F1 fanglomerate. This surface can be correlated with the gently sloping regional depositional surface on the Vathyrkakas plateau and adjacent hills. The F2 channels developed later at lower topographic levels, in response to glacio-eustatically controlled incision during continuing surface tectonic uplift. RSL fell between F1 and F2 times (Poole and Robertson, 1991), which caused down-cutting to a lower base-level. Fanglomerates of this age are exposed on the valley sides of the Dhiarzos river, tens of metres above the present valley floor. A good example is exposed on the road NW from Kouklia village down to the concrete bridge over the Dhiarzos. The regional erosion surface that extends south of Kouklia, and to the southwest towards Paphos, defines the extensive coastal plain in that existed in F2 times, and that was subsequently preserved due to uplift.

The progressive uplift, and subsequent incision, of the Troodos Massif and its sedimentary cover, resulted in a change in the nature of the bed-load through the fanglomerate series with time. The earliest fanglomerates (F1 and F2) are dominated by Troodos material with abundant gabbro boulders; whereas the later fanglomerates (F3, F4 and the proto-Dhiarzos and its tributaries) are dominated by material derived from a higher structural level in the Troodos ophiolite (i.e. diorites from the sheeted dyke complex), the Mamonia Complex, and chalks from the Troodos sedimentary cover.

The present-day drainage network of the Dhiarzos river and its tributaries was established by F3 times; this ‘initial topography’ developed in response to further uplift, combined with slightly lower base-levels related to eustatic sea-level fall (Poole and Robertson, 1991). Poole and Robertson (1998) correlate the F3 Fanglomerate unit with littoral marine terraces in southwestern, southern and southeast Cyprus (e.g. the low-lying coastal plain at an altitude of 8-11 m above mean sea level in the Paphos region), dated at 185-219 ka, and associated with the marine highstand that correlates with oxygen isotope substance 7e (Poole et al., 1990). The evidence that the ‘initial topography’ developed no later than F3 times is thus: at present, the bedrock geology in the lower reaches of the Aragin Vathin river is the Pakhna Formation, and in it upper reaches the Lefkara Formation (in the vicinity of the Oreites wind farm). The northern limit of the elevated Oreites Forest block is a drainage divide (**Figs 11 & 12**). Therefore, at present the Aragin Vathin river and its tributaries do link into the river network that drains the Troodos Massif to the north of village of Archimandrita. The presence of material derived from the Troodos massif in F1 and F2 terrace deposits in the vinicity of Souskiou-Laona suggests that the regions were once connected. The proto-Dhiarzos river must have captured the drainage network north of Archimandrita in between F2 and F3 times, meaning that sediment derived from the Troodos then bypassed the ravine.

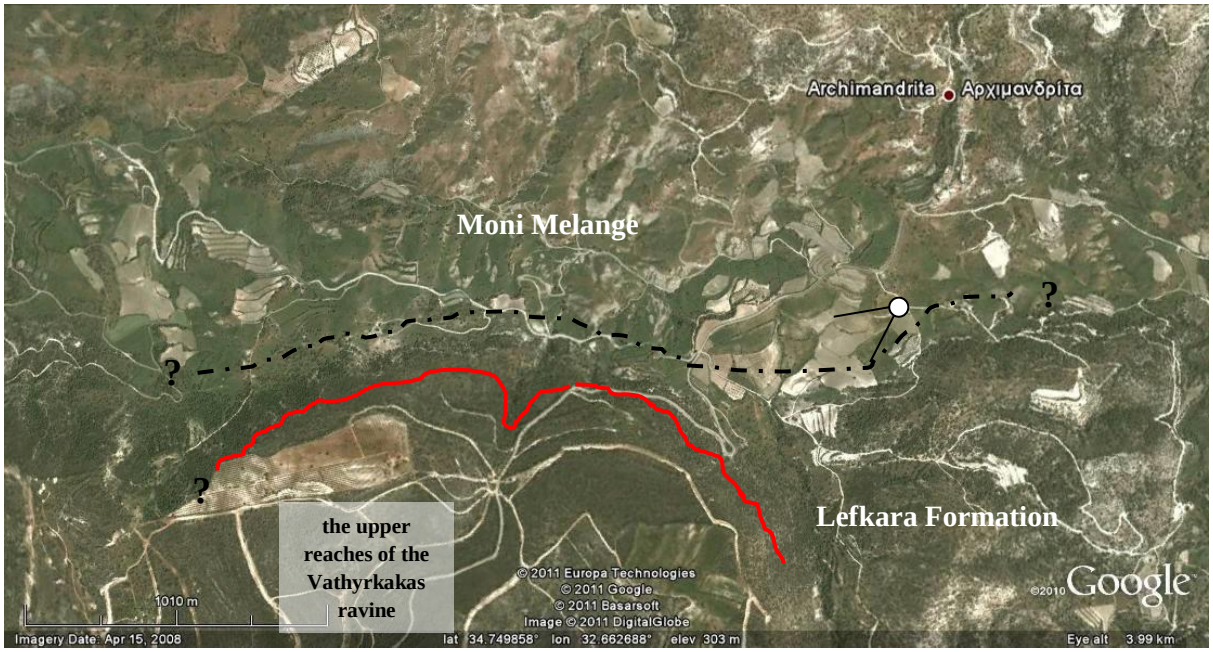

Figure 11: Satellite image of the region around Archimandrita (reproduced from Google Earth), showing the geological boundary between the Lefkara Formation and the Moni Melange (black dashed line) and the watershed at the northern limit of the elevated Oreites Forest block (red line). The photograph shown in figure 12 was taken from the vantage position marked by the closed white circle.

Figure 12: View south from Archimandrita village, looking at the northern slopes of the topographically elevated Orietes Forest block (marked by the wind turbines). The Dhiarzos river is located in the larger valley, which runs perpendicular to our viewpoint, in the centre of the photograph. The line of wind turbines approximately delineate the drainage divide between the Aragin Vathin drainage network, and the Archimandrita drainage network, which feds the Dhiarzos river.

The few pebbles of Troodos-derived material that are found in the terrace deposits within the ravine are believed to be reworked from earlier fanglomerate units.

The incision history of the Vathyrkakas ravine

The Vathyrkakas ravine is cut into the Vathyrkakas-Laona plateau, which is correlated with the regional F1 erosion surface, so the ravine must be F2 age or younger. In the chronological framework of Poole and Robertson (1991) this indicates that initial incision occurred in the Latest Pliocene/Early Pleistocene. The topography of the Vathyrkakas plateau, the Vathyrkakas ravine, and the Dhiarzos river were therefore well established by the archaeological period of interest.

The questions remains as to the extent the ravine, and its slopes, were modified in Chalcolithic times. To answer this question, we must examine the geomorphology of the ravine, specifically where the Aragin Vathin river exits to the main Dhiarzos channel. At the channel exit, the ravine hangs 2 m

above the present level of the Dhiarzos river bed. Immediately to the south of the channel exit, the present Dhiarzos river channel is incised into chalks of the Pakhna Formation, forming a 5-6 m cliff. A prominent large field occurs at the height of the 6 m high cliff, which may be a relict fluvial terrace, albeit modified. If so, given its topographic elevation relative to the present Dhiarzos base-level, it may correlate with Poole and Robertson's (1991; 1998) F3 fanglomerate unit. At the channel exit, there is a thick accumulation (6m) of interbedded colluvial and alluvial sediment; the top of this accumulation corresponds to the level of the 6m terrace. The colluvial layers are characterised by poorly to moderately stratified, internally disorganised, matrix-supported cobble to pebble conglomerates. Clasts are poorly sorted, immature, sub-angular to sub-rounded, and are dominated by chalk and calcarenite. In contrast, the alluvial layers are confined to channelized features and small lenticular lenses, and are comprised of moderately stratified, graded, matrix-supported pebble conglomerates, with some clast imbrication. The clasts are derived from the adjacent bedrock.

The youngest incision event in the immediate area is the incision of the Dhiarzos river to its present level. The ravine was evidently cut earlier, down to the +2m surface but not significantly any deeper, as it is now essentially a hanging valley. This implies that at the time the ravine was being cut down to its present level, the discharge from the ravine was negligible. To constrain the age at which the Vathyrkakas fan built out from the ravine, a number of samples were collected through the fan deposits for optically stimulated luminescence (OSL) analysis (Appendix A). Given the dimensions of the fan it was not possible to sample from the base, therefore it is only the later part of the evolution of the fan that is constrained by the OSL dating. The dates obtained by the OSL method are intriguing: sediments near the mouth of the ravine are dated from the fourth to second century BC to the Ventian period. This implies that sediment was being flushed through the ravine relatively late in the history, long after the ravine was first cut. Note, we're not implying that the ravine was cut at this time; simply that flows within the ravine were sufficient to move material down the ravine and deposit it at the mouth, during intensified climatic events. This observation explains the near absence of Troodos-derived material in the younger channel fills within the ravine, as this material is likely to have been flushed through the ravine in multiple events; it also explains the absence of Chalcolithic debris at the base of the ravine, as this material would also have been flushed through the ravine prior to the 1st century BC.

Slope stability

The settlement on the Laona ridge is located on the precipitous northwestern slope of the Vathyrkakas ravine. The northwestern slope has a 'stepped profile', with hard competent bands of calcarenite and chalk, which form prominent ridges, and weaker, less competent bands of marl. The latter are more prone to weathering than the former. The bedrock in the vicinity of the excavation consists of several rock types, which have an influence on the ground surface: (i) exposed Pakhna Formation calcarenites, which are very poorly vegetated, and (ii) poorly exposed Pakhna Formation marls, which form lumpy, disturbed and vegetated ground.

The settlement itself, occupies a position, on/above a slumped unit of chalks and marls, underlain by an inferred detachment surface, and backed by a break-away fracture. The occupants of the Chalcolithic site exploited the bedrock geology, excavating through the softer marl to obtain calcarenite, to secure foundations for their buildings. At present, there is no constraint on the age of the inferred fault inward of the Souskiou-Laona settlement: it may be that the fault was cut in geological time (the trend of the inferred fault is sub-parallel to faults observed cutting the bedrock geology), or that the fault was cut later in Pleistocene or Recent times (through the reactivation of older structures).

It is believed that the slopes above the *Vathyrkakas* ravine have been constantly evolving since the ravine was first cut. It is known that the slope has evolved since Chalcolithic time - due to the excavation of buildings that would have originally extended outward into the ravine from their present position. Indeed, it would appear that the slope was evolving during the Chalcolithic period of occupation, as the current excavation has shown the interdigitation of colluvial and anthropogenic horizons. We would argue that slope failures have occurred intermittently at the site, perhaps triggered by earthquakes, from the time of occupation to the present day, resulting in parts of the settlement slipping into the ravine on new detachment surfaces or re-activated old ones. It is not implied that the whole ravine was cut in post-Chalcolithic times; rather that, the original river-cut scarps are not stable.

OSL investigations at the excavation support this hypothesis (Appendix A): (i) luminescence screening measurements performed on site using portable OSL instruments, coupled with in-situ gamma spectrometry, indicate that the interbedded colluvial and anthropogenic layers share similar IRSL and OSL net signal intensities, suggesting that these units accumulated within a similar time period; and (ii) calibrated luminescence screening measurements made using a simplified single aliquot dose procedure on paired aliquots of HF-etched quartz and polymineral separates, provide some preliminary stored dose information. The interbedded colluvial/anthropogenic layers at the base of section 133 (profile 3; Appendix A) contain a range of materials, with variable luminescence sensitivities, and variable IRSL, OSL and TL residuals, as reflected in heterogeneous stored dose estimates (C-1). If an estimate of the natural radioactivity of the sediment is made, based on the high resolution gamma spectrometry (HRGS) and thick source beta counting (TSBC) results from the Dhiarzos section, coupled with the in situ gamma dose rate measurements taken through the site, then a preliminary chronology is established: (i) the stored dose estimates at the base of the section correspond to ages in the Late Chalcolithic to Early Bronze Age; (ii) the stored dose estimates at the top of the section correspond to ages in the 15th and 20th centuries. Rogers and Algermissen (2003) have compiled a list of historical earthquakes to have affected central Cyprus in the period 1303 AD to 2001 AD: interestingly the dates obtained for the upper colluvial units, 1499 ± 50 AD and 1930 ± 40 AD, are synchronous with documented earthquakes in 1491 (magnitude 8) and 1933 (magnitude 4).

6. References

Aitken, M.J., 1983, Dose rate data in SI units: PACT, v. 9, p. 69–76.

Bøtter-Jensen, L., Bulur, E., Duller, G.A.T., and Murray, A.S., 2000, Advances in luminescence instrument systems: Radiation Measurements, v. 32, p. 523-528.

Eaton, S., and Robertson, A., 1993, The Miocene Pakhna Formation, southern Cyprus and its relationship to the Neogene tectonic evolution of the Eastern Mediterranean: Sedimentary Geology, v. 86, p. 273-296.

Kähler, G., and Stow, D.A.V., 1998, Turbidites and contourites of the Palaeogene Lefkara Formation, southern Cyprus: Sedimentary Geology, v. 115, p. 215-231.

Kinnaird, T.C., and Robertson, A.H.F., 2012, Tectonic and sedimentary response to incipient diachronous collision of the African and Eurasian plates in southern Cyprus, easternmost Mediterranean region, *in* Robertson, A.H.F., Parlak, O., and Ünlügenç, U., eds., Geological Development of the Anatolia and Environs, Journal of the Geological, Special Publication.

Kinnaird, T.C., Robertson, A.H.F., and Morris, A., 2011, Timing of uplift of the Troodos Massif (Cyprus) constrained by sedimentary and magnetic polarity evidence: Journal of the Geological Society, v. 168, p. 457-470.

Mejdahl, V., 1979, Thermoluminescence daing: Beta-dose attenuation in quartz grains Archaeometry, v. 21, p. 61-72.

Murray, A.S., and Wintle, A.G., 2000, Luminescence dating of quartz using an improved single-aliquot regenerative-dose protocol: Radiation Measurements, v. 32, p. 57-73.

NEA, 2000, The JEF-2.2 Nuclear Data Library: Nuclear Energy Agency, Organisation for economic Co-operation and Development. JEFF Report, v. 17.

Poole, A.J., and Robertson, A.H.F., 1991, Quaternary uplift and sea-level change at an active plate boundary, Cyprus: Journal of the Geological Society of London, v. 148, p. 909-921.

—, 1998, Pleistocene fanglomerates deposition related to uplift of the Troodos Ophiolite, Cyprus, *in* Robertson, A.H.F., Emeis, K.-C., Richter, C., and Camerlenghi, A., eds., Proceedings ODP Scientific Results, Volume 160, p. 544-558.

—, 2000, Quaternary marine terraces and aeolinites in coastal south and west Cyprus: implications for regional uplift and sea-level change, *in* Panayides, I., Xenophontos, C., and Malpas, J., eds., Proceedings of the Third Internal Conference on the geology of the Eastern Mediterranean, Volume 160, Cyprus Geological Survey Department, p. 544-568.

Poole, A.J., Shimmield, G.B., and Robertson, A.H.F., 1990, Late Quaternary uplift of the Troodos Ophiolite, Cyprus; uranium-series dating of Pleistocene coral: Geology, v. 18, p. 894-897.

Prescott, J.R., and Hutton, J.T., 1994, Cosmic ray contributions to dose rates for luminescence and ESR dating: Large depths and long-term time variations: Radiation Measurements, v. 23, p. 497-500.

Rogers, A.M., and Algermissen, S.T., 2003, An earthquake hazard assessment of Cyprus, *in* Petrides, G., Chrysostomou, C., Kyrou, K., and Hadjigeorgiou, C., eds., Proceedings: Earthquake Risk Minimization; International conference.

Appendix A: Optically stimulated luminescence investigations at Souskiou-Laona, Cyprus

A. Introduction

This report is concerned with optically stimulated luminescence (OSL) investigations of sediment samples collected from the University of Edinburgh excavations at Sousikou-Laona, Cyprus. Fieldwork was undertaken in April 2011 to retrieve sediment samples from key features to be used in assessing the suitability of the material for OSL dating, and to provide material for OSL dating analyses during post-excavation stages.

B. Sampling

T.C. Kinnaird visited the University of Edinburgh excavation at Souskiou-Laona, Cyprus, in May 2011 to collect samples for OSL dating and profiling. A list of the samples collected for OSL dating is given in table B-1. The samples denoted by an '*' were approved by E. Peltenburg for dating/profiling.

Profile no.	Context no.	Height beneath datum	Description	Question?
Profile 1: N34°43.599', E32°35.236				
P1/1	1142	15	colluvium	to constrain interaction between periods of slope instability and settlement
P1/2	1142	25	colluvium	
P1/3	1142	27	colluvium	
P1/4	1143	45	anthropogenic horizon	
P1/5	-	68	colluvium	
P1/6	-	-	colluvium	
Profile 2: N34°43.602', E32°35.226				
P2/1	658	24	slopewash	interaction between periods of slope instability and settlement
P2/2	1142	35	slopewash	
P2/3	1142	46	inc. occupation layers	
P2/4	1143	57	inc. occupation layers	
P2/5	-	71	occupation unit	
Profile 3: N34°43.604', E32°35.245 Section no. 185				
P3/1 *	559	50	colluvium	interaction between periods of slope instability and settlement
P3/2 *	781	70	colluvium	
P3/3 *	767	114	colluvium	
P3/4 *	767	122	colluvium	
P3/5 *	767	135	anthropogenic horizon	
Section no. 133				
P3/6 *	928	115	anthropogenic layer?	interaction between periods of slope instability and settlement; re-build of northern wall
P3/7 *	910	28	foundation wall	
P3/8 *	1084	50	foundation wall	
Profile 4: N34°43.599', E32°35.240'				
P4/1	559	8	midden deposit?	terminus post quem of construction - building 897
P4/2	1038	24	midden deposit?	
P4/3	1038	42	midden deposit?	
P4/4	1038	73	midden deposit?	
Profile 5: N34°43.436', E32°34.703'				
P5/1*	-	210	fluvial sediments	interpret history of the

P5/2*	-	420	fluvial sediments	*Vathyrkakas* ravine
P5/3*	-	640	fluvial sediments	
OSL1*	-	220	fluvial sediments	
OSL2*	-	430	fluvial sediments	
OSL3*	-	650	fluvial sediments	

Table B-1: Sample Numbers/Context Numbers. Samples submitted for dating are denoted by an *.

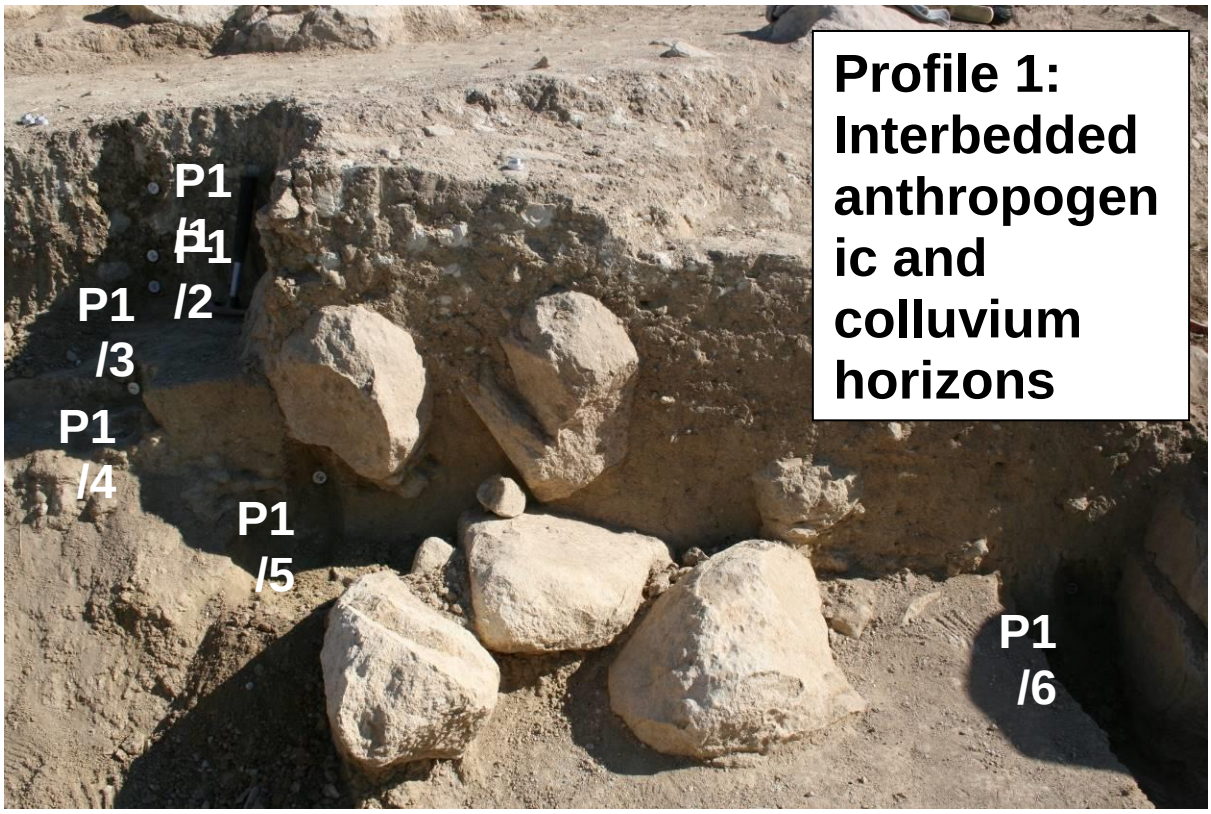

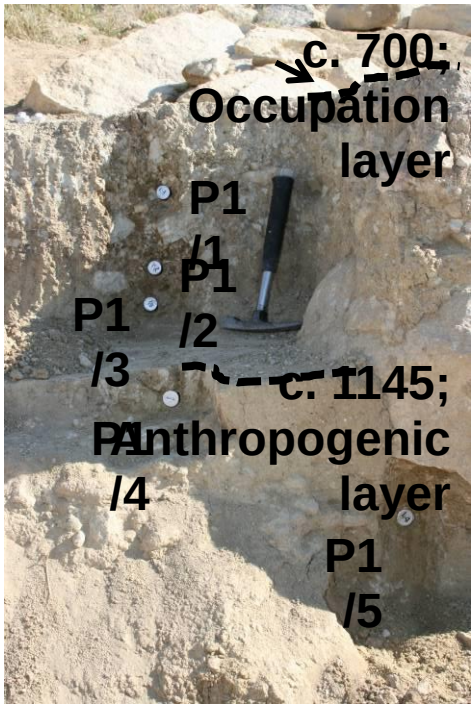

Profile 1: N34°43.599', E32°35.236			
Profile no.	Context no.	Height beneath datum	Interpretation
P1/1	1142	15	Colluvium
P1/2	1142	25	Colluvium
P1/3	1142	27	Colluvium
P1/4	1143	45	Anthropogenic horizon
P1/5	-	68	Colluvium
P1/6	-	-	Colluvium

Figure B-1: Profile 1, interbedded anthropogenic and colluvium horizons

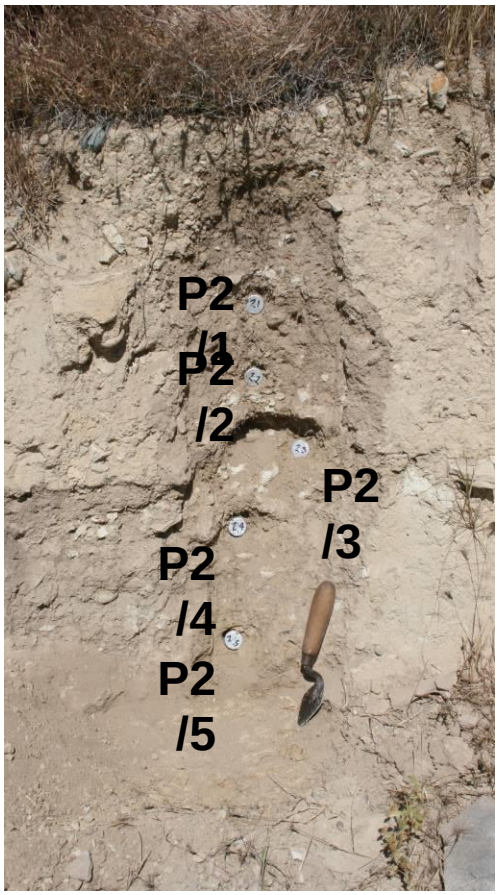

Profile 2: Colluvium

Profile 2: N34°43.602', E32°35.226			
Profile no.	Context no.	Height beneath datum	Interpretation
P2/1	658	24	slopewash
P2/2	1142	35	slopewash
P2/3	1142	46	inc. occupation layers
P2/4	1143	57	inc. occupation layers
P2/5	-	71	occupation unit

Figure B-2: Profile 2, colluvial horizons containing Chalcolithic detritus

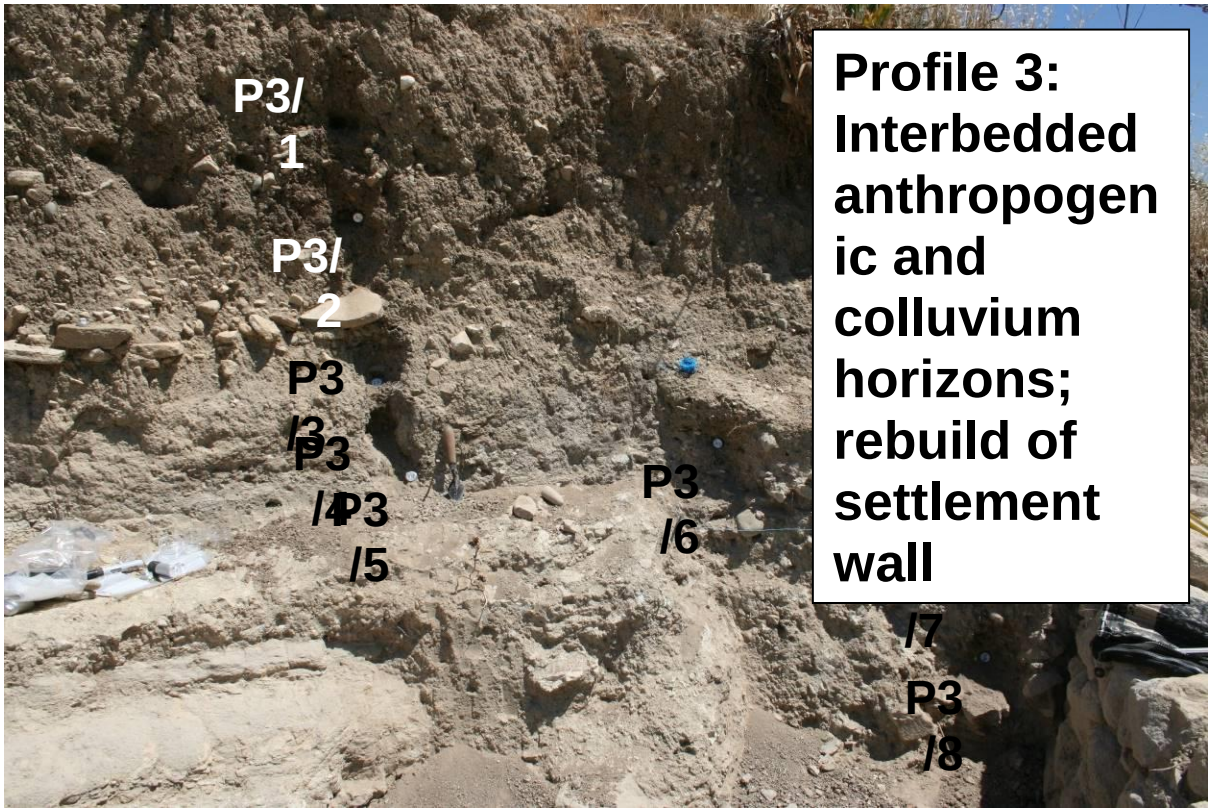

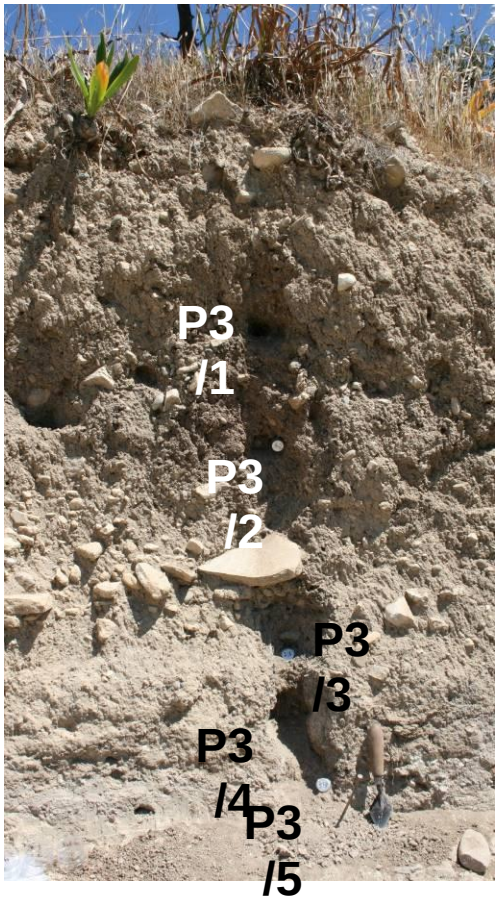

Profile 3: Interbedded anthropogenic and

Profile 3: Section no. 185			
Profile no.	Context no.	Height beneath datum	Interpretation
P3/1	559	50	colluvium
P3/2	781	70	colluvium
P3/3	767	114	colluvium
P3/4	767	122	colluvium
P3/5	767	135	anthropogenic layer
Section no. 133			
P3/6	928	115	anthropogenic layer?
P3/7	910	28	foundation wall
P3/8	1084	50	foundation wall

Figure B-3: Profile 3, interbedded colluvial and anthropogenic horizons

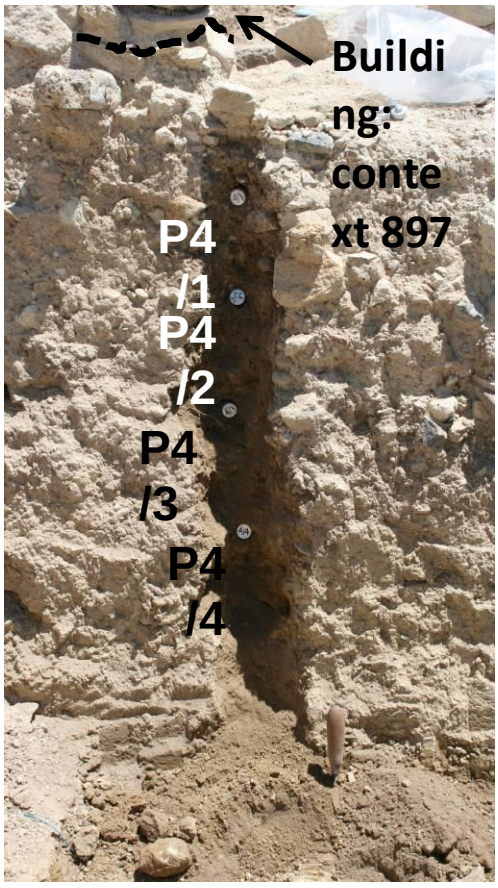

Profile 4: colluvium beneath settlement

Profile 4:			
Profile no.	Context no.	Height beneath datum	Interpretation
P4/1	559	8	midden deposit?
P4/2	1038	24	midden deposit?
P4/3	1038	42	midden deposit?
P4/4	1038	73	midden deposit?

Figure B-4: Profile 4, colluvium beneath Chalcolithic structure

Figure B-5: Profile 5, Vathyrkakas fan/Dhiarzos terrace

26 profiling samples were collected from five profiles. Profiles 1 - 3 were taken through interbedded occupation, anthropogenic and colluvial layers in the Souskiou-Laona excavation. Profile 4 was taken through the substrate to building 897. Profile 5 is taken through the sediments that comprise the Vathyrkakas alluvial fan, at the intersection of the Vathyrkakas ravine, and the main Dhiarzos river channel. 3 OSL dating samples were collected through this profile, to provide a chronological framework to interpret the later landscape history of the Vathyrkakas ravine.

B.1 In-situ field gamma spectrometry measurements

Field gamma spectrometry (FGS) measurements were made using a Health Physics Instruments Rainbow MCA with a 2"x 2" NaI probe. Prior to fieldwork, measurements were made using this system on the doped concrete reference pads at SUERC in order to provide cross-reference to dose-rate conversion factors established by Sanderson in 1986, based on comparisons with TL dosimetry in doped blocks then at the Oxford and Risø luminescence laboratories. The spectra were calibrated to the 1457 keV peak from ^{40}K, then dose rates were determined from integral counts >450 keV, >1350 keV, and the energy integral (sum of counts times energy) across all the recorded spectrum. Using this approach, dose rates from the pads were reproduced that were within error of expected values.

Field spectra were each measured for 300s in positions at the top and bottom of the studied profiles, and in holes cut around the luminescence sampling positions using a towel, and calibrated to the 1461 keV peak from ^{40}K before calculation of dose rates. Table B-2 shows the mean gamma dose rates recorded in-situ for the dating samples.

Profile No.	SUTL No.	Field gamma (wet), (mGy a^{-1})
1	2378	0.36 ± 0.03
2	2379A	0.28 ± 0.15
	2379E	0.43 ± 0.04
3	2380A	0.29 ± 0.03
	2380E	0.29 ± 0.03
4	2381	0.28 ± 0.03
5	2385A	0.38 ± 0.03
	2385C	0.34 ± 0.03
	2382	0.38 ± 0.03
	2384	0.34 ± 0.03

Table B-2: In situ gamma dose rates measurements made using a Health Physics Instruments Rainbow MCA with a 2"x 2" NaI probe

B.2 Field profiling measurements

Field profiling measurements were made using a SUERC portable OSL reader, equipped with blue LEDs emitting around 470 nm and a U340 detection filter pack to detect in the region 270-380 nm, while cutting out stimulating light. Samples were presented as bulk sediment in 50mm plastic petri dishes. Natural luminescence signals were measured following an interleaved sequence of system dark count (background), infra-red stimulated luminescence and optically stimulated luminescence, similar to that described by Sanderson and Murphy (2010).

The results of the field profiling are shown in figures B-6 to B-9. Profile 1, 2 and 3 were taken to establish the relationship between periods of occupation and slope instability: specifically, to determine whether periods of slope instability and occupation were contemporaneous.

In profile 1, shown in figure B-6, the anthropogenic horizon has similar OSL net signal intensities to the substrate which it overlies, possibly suggesting that the two horizons are near equivalent in age. It is also notable that the IRSL/OSL ratio for the anthropogenic and underlying colluvial deposits are similar, implying that the mineralogy of the two units is comparable. Further up the section, IRSL and OSL net signal intensities are higher, indicating that the material above the anthropogenic layer contains larger residual signals, implying that it was not completely reset on deposition. The sample taken from the near surface has a high IRSL/OSL ratio, which may be indicative of a greater ratio of feldspar to quartz ratio in this unit, with less experience of oxidation weathering in comparison to the lower deposits.

Figure B-7 shows the profile associated with the cut bedrock feature in the southwest of the excavation, the occupation unit (context 744) associated with it and the colluvial deposits that overlie it (contexts 678/659 and 658). The occupational unit associated with the cut bedrock feature has comparable IRSL and OSL net signal intensities to those obtained for the anthropogenic horizon in profile 1. Interestingly, the two colluvial layers immediately above this unit, which contain some occupational detritus, have similar signal intensities. IRSL and OSL depletion ratios within these units are moderately high, implying that the material was well-bleached prior to deposition, and show promising behaviours for luminescence dating. As in profile 1, the colluvial deposits immediately above the 'occupational layers', show high signal intensities, suggesting that this material contains larger residual doses, and that the material was not completely reset on deposition.

The profile shown in figure B-8 encompasses a sequence of interbedded colluvial and anthropenogic layers to the northeast of the northwestern structure, and the foundation of the northwestern structure. The material at the base of the profile, in contexts 910 and 1084, has large IRSL and OSL net signal intensities, comparable to those obtained for the anthropogenic horizon in profile 1. Further up the profile, there is a progressive decrease in luminescence signals through the interbedded colluvial/ anthropogenic layers and into the most recent deposits. In-situ dose rate measurements indicate that the environmental radioactivity of the samples at 50 cm and 135 cm depth in the section are comparable. Therefore, the net signal intensities may be taken as a proxy for age, with the lower signal intensities implying that the upper units are younger. The net signal intensities for the interbedded colluvial/anthropenogenic horizons are comparable, suggesting that these units are near synchronous in age. It is interesting that the two upper units in the profile, yield low IRSL and OSL signal intensities, implying that the material has a 'zero' age, which suggests that the modern soil surface continues to be instability to the present day.

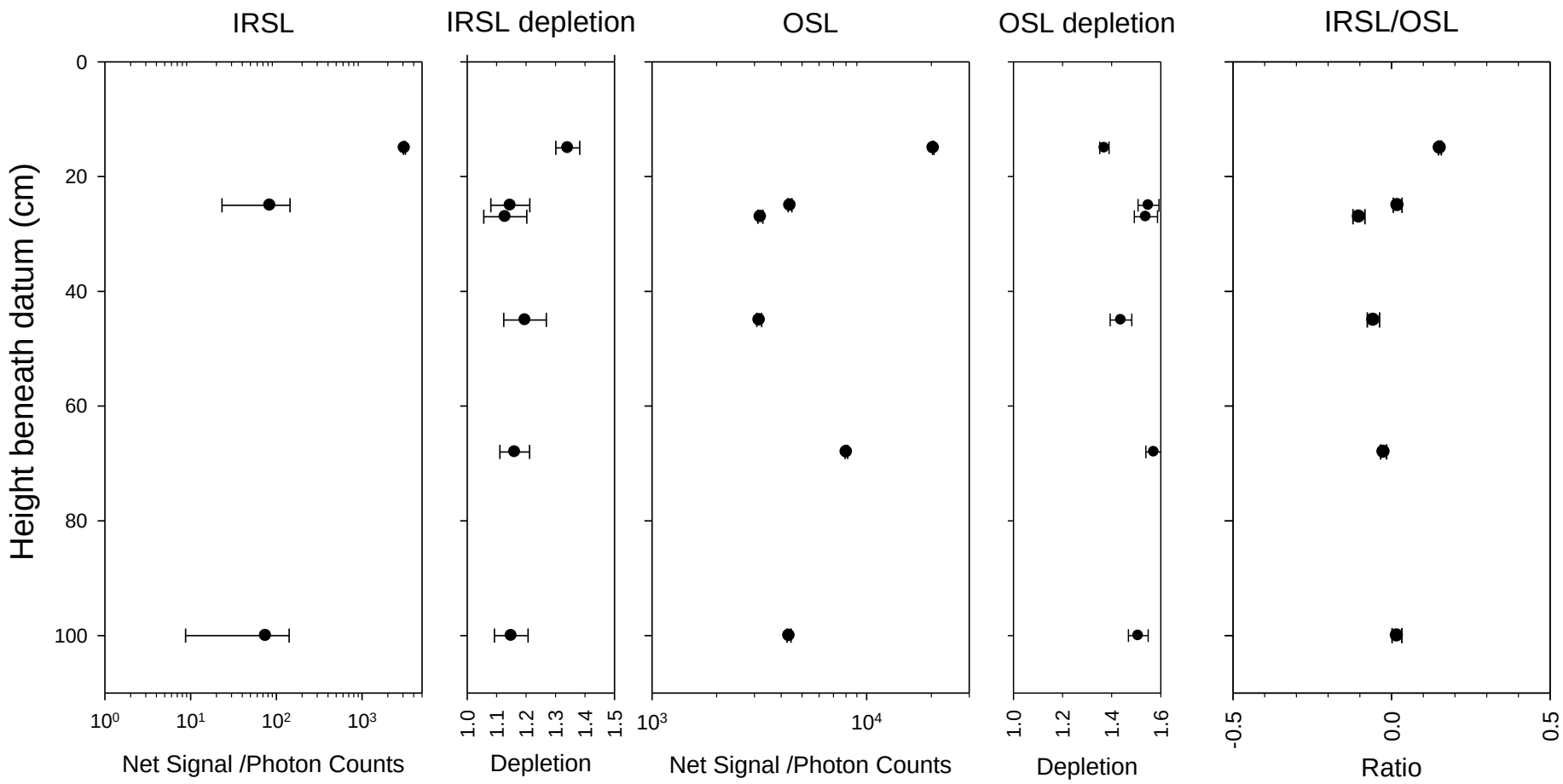

Figure B-6: Luminescence measurements made using the SUERC portable OSL reader, Profile 1

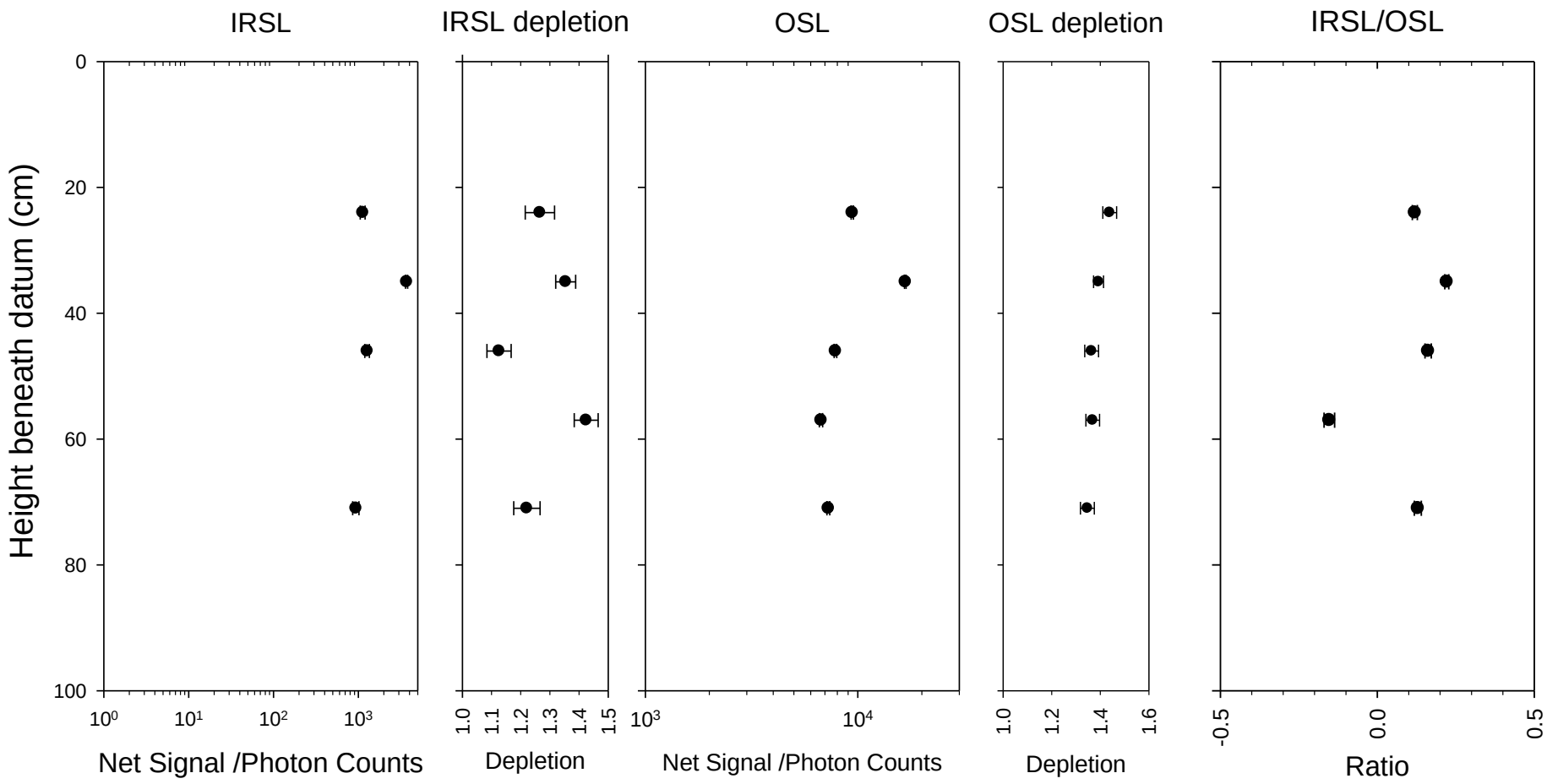

Figure B-7: Luminescence measurements made using the SUERC portable OSL reader, Profile 2

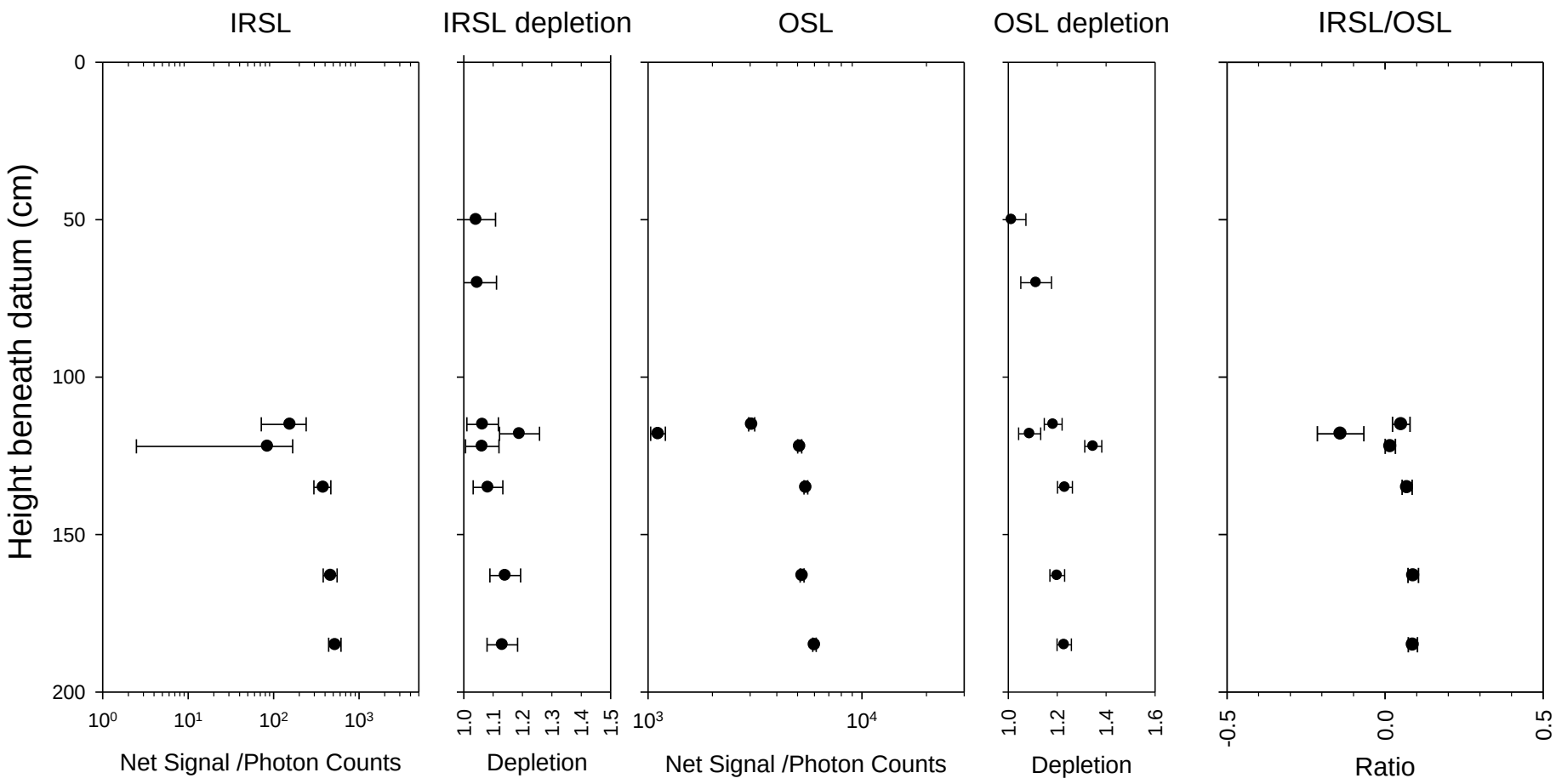

Figure B-8: Luminescence measurements made using the SUERC portable OSL reader, Profile 3

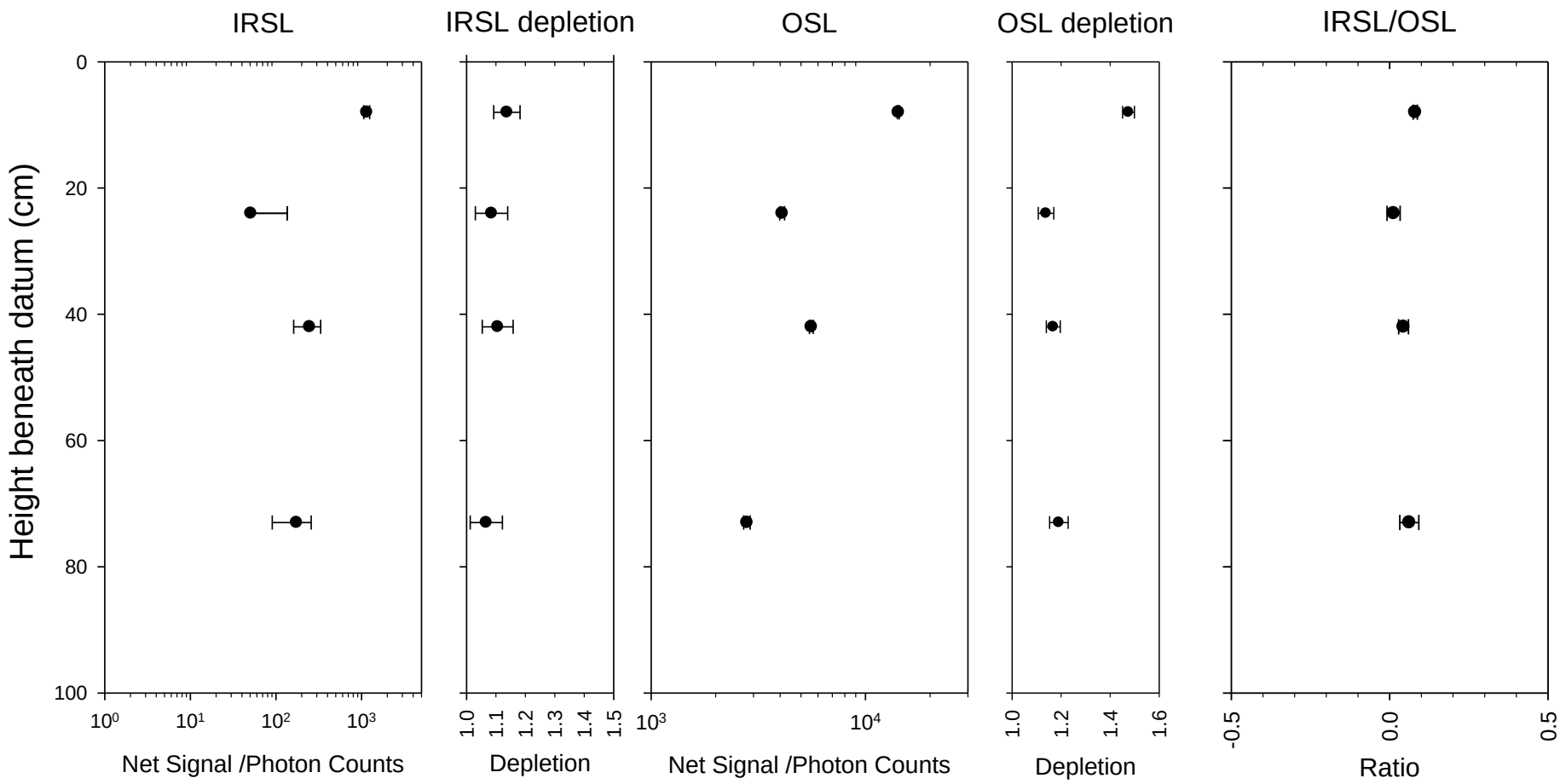

Figure B-9: Luminescence measurements made using the SUERC portable OSL reader, Profile 4

C. Luminescence screening measurements

C.1 Sample preparation

All sample handling and preparation was conducted under safelight conditions in the SUERC luminescence dating laboratories. Material from each profiling sample was wet sieved to extract the 90-250 μm sized fraction, which was treated with 1M HCl for 10 minutes to dissolve carbonates. The samples were then treated with 15% HF for 15 minutes to dissolve the less chemically resistant minerals and to etch the outer part of the grains (followed by a 1M HCl treatment for 10 minutes). Each sample was then split into two sub-samples, one for polymineral analysis and one for quartz analysis. The quartz subsample was treated with 40% HF for 40 minutes, and then treated with 1 M HCl for 10 minutes. The samples were dried at 50°C and transferred to Eppendorf tubes for storage. Two polymineral and two quartz aliquots were then prepared for each sample; grains were dispensed onto 1cm diameter stainless steel disks, using silicon grease for adhesion.

C.2 Analytical procedure

Luminescence sensitivities (photon counts per Gy) and stored doses (Gy) were evaluated from paired aliquots of the HF-etched quartz and polymineral fractions, using Risø D-15 automatic readers (equipped with a $^{90}Sr/^{90}Y$ β-source for irradiation, blue LEDs emitting around 470 nm and infrared (laser) diodes emitting around 830 nm for optical stimulation, and a U340 detection filter pack to detect in the region 270-380 nm, while cutting out stimulating light; Bøtter-Jensen et al. 2000) and a simplified SAR protocol. In this protocol, the readout cycle consists of a natural measurement, followed by a nominal 1Gy test dose, and a nominal 5Gy regenerative dose with readout with 1Gy test dose. For the quartz samples, a 240˚C preheat was used with 60s OSL measurements using the blue LEDs. For the polymineral samples, a 260˚C preheat was followed by 60s OSL measurements using the IR LEDs at 50˚C, an OSL measurement taken at 125˚C, again for 60s, and a TL measurement to 500˚C.

C.3 Results

The results are presented as dose-depth and sensitivity-depth profiles in figures C-1 to C-2. Laboratory luminescence screening results from profile 3 reproduce the apparent trends/maxima observed in the field profiling data set (Figs B-1 and C-1). Material at the base of section 185 (the foundation trench) yielded luminescence sensitivities in the range ~ 1500 to 6000 photons per Gy, and stored dose values in the range ~ 3.5 to 4 Gy. The interbedded colluvial/anthropogenic layers at the base of section 133 contain a range of materials, with variable luminescence sensitivities, and variable IRSL, OSL and TL residuals, as reflected in heterogeneous stored dose estimates (C-1). In contrast, the two profiling samples from the top of the section (133), yielded luminescence sensitivities in the range 700 to 3000 photons per Gy, and stored doses in the range 0.4 Gy to near zero. This confirms the relative chronology established by the field profiling measurements: i.e. an early period, when slope failures were common, coeval with the occupation of the site, a hiatus in deposition, then a later episode of slope failures. If an estimate of the natural radioactivity of the sediment is made, based on the HRGS and TSBC results from the Dhiarzos section, and in situ gamma dose rate measurements taken through this profile, stored dose estimates for the lower unit correspond to ages in the Mid Chalcolithic to Early Bronze Age. Stored dose estimates for the lower flow in the upper unit correspond to an age approximately 1500 AD, and for the upper flow c. 1930 AD.

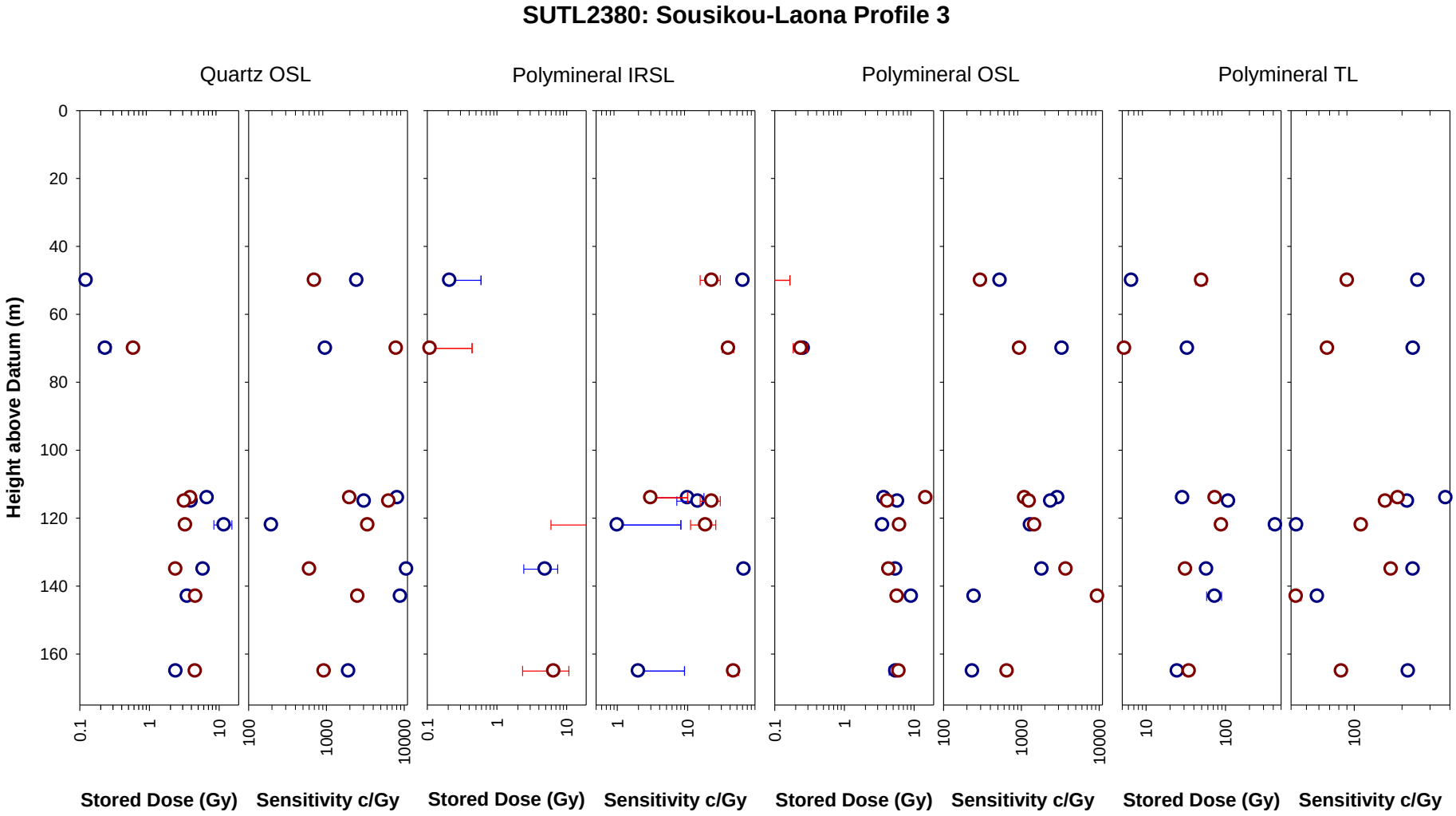

Figure C-1: Luminescence profiling/screening measurements from profile 3

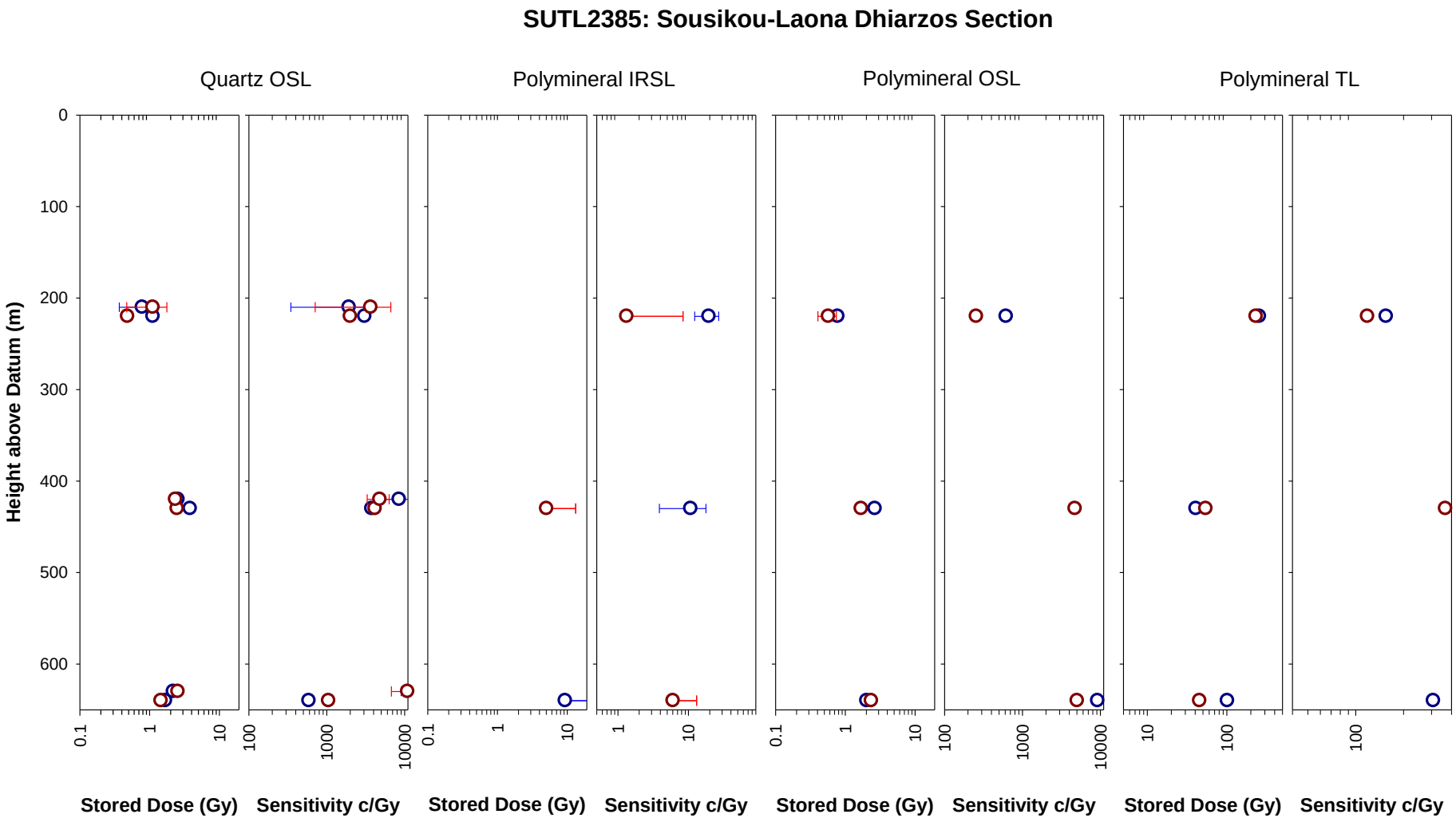

Figure C-2: Luminescence profiling/screening measurements from the Dhiarzos river section

D. Laboratory Dose Rate Measurements

D.1 Analytical procedure

Dose rates were measured in the laboratory using high resolution gamma spectrometry (HRGS) and thick source beta counting (TSBC). HRGS measurements were performed using a 50% relative efficiency "n" type hyper-pure Ge detector (EG&G Ortec Gamma-X) operated in a low background lead shield with a copper liner. Gamma ray spectra were recorded over the 30 keV to 3 MeV range from each sample, interleaved with background measurements and measurements from SUERC Shap Granite standard in the same geometries. Counting times of 80ks per sample were used. The spectra were analysed to determine count rates from the major line emissions from ^{40}K (1461 keV), and from selected nuclides in the U decay series (^{234}Th, ^{226}Ra + ^{235}U, ^{214}Pb, ^{214}Bi and ^{210}Pb) and the Th decay series (^{228}Ac, ^{212}Pb, ^{208}Tl) and their statistical counting uncertainties. Net rates and activity concentrations for each of these nuclides were determined relative to Shap Granite by weighted combination of the individual lines for each nuclide. The internal consistency of nuclide specific estimates for U and Th decay series nuclides was assessed relative to measurement precision, and weighted combinations used to estimate mean activity concentrations (Bq kg^{-1}) and elemental concentrations (% K and ppm U, Th) for the parent activity. These data were used to determine infinite matrix dose rates for alpha, beta and gamma radiation.

Beta dose rates were also measured directly using the SUERC TSBC system (Sanderson, 1988). Sample count rates were determined with six replicate 600 s counts for each sample, bracketed by background measurements and sensitivity determinations using the Shap Granite secondary reference material. Infinite-matrix dose rates were calculated by scaling the net count rates of samples and reference material to the working beta dose rate of the Shap Granite (6.25 ± 0.03 mGy a^{-1}). The estimated errors combine counting statistics, observed variance and the uncertainty on the reference value.

The dose rate measurements were used in combination with the assumed burial water contents, to determine the overall effective dose rates for age estimation. A cosmic dose rate of 0.17 ± 0.01 mGy a^{-1} has been calculated for the latitude of the sampling locations, using the method of Prescott and Hutton (1994).

D.2 Results

HRGS results are shown in Table D-1, both as activity concentrations (i.e. disintegrations per second per kilogram) and as equivalent parent element concentrations (in % and ppm), based in the case of U and Th on combining nuclide specific data assuming decay series equilibrium. Infinite matrix alpha, beta and gamma dose rates from HRGS are listed in Table D-2, together with infinite matrix beta dose rates from TSBC.

The water content measurements with assumed values for the average water content during burial are given in Table D-3. The table also lists the gamma dose rate from the HRGS after application of a water content correction. Effective dose rates to the HF etched 200 μm quartz grains are given for the gamma dose rate and beta dose rate (the mean of the TSBC and HRGS data, accounting for water content and grain size).

SUTL no.	Activity Concentration (Bq kg^{-1})[a]			Equivalent Concentration[b]		
	^{40}K	U	Th	K (%)	U (ppm)	Th (ppm)
2382	181 ± 13	30 ± 2	9 ± 1	0.58 ± 0.04	2.45 ± 0.16	2.25 ± 0.29
2383	193 ± 13	25 ± 2	7 ± 1	0.62 ± 0.04	2.05 ± 0.14	1.75 ± 0.28
2384	166 ± 13	14 ± 1	9 ± 1	0.54 ± 0.04	1.11 ± 0.11	2.33 ± 0.27

Table D-1: Activity and equivalent concentrations of K, U and Th determined by HRGS

[a]Shap granite reference, working values determined by David Sanderson in 1986, based on HRGS relative to CANMET and NBL standards.

[b]Activity and equivalent concentrations for U, Th and K determined by HRGS (Conversion factors based on NEA (2000) decay constants): 40K: 309.3 Bq kg^{-1} %K^{-1}, 238U: 12.35 Bq kg^{-1} ppmU^{-1}, 232Th: 4.057 Bq kg^{-1} ppmTh^{-1}.

SUTL no.	HRGS, dry (mGy a^{-1})[a]			TSBC, dry (mGy a^{-1})	Field gamma, wet (mGy a^{-1})
	Alpha	Beta	Gamma		
2382	8.48 ± 0.51	0.91 ± 0.04	0.54 ± 0.03	0.82 ± 0.04	0.38 ± 0.03
2383	7.00 ± 0.44	0.87 ± 0.04	0.48 ± 0.02	0.83 ± 0.04	0.36 ± 0.05
2384	4.82 ± 0.36	0.68 ± 0.04	0.38 ± 0.02	0.81 ± 0.05	0.34 ± 0.03

Table D-2: Infinite matrix dose rates determined by FGS, HRGS and TSBC.

[a]based on dose rate conversion factors in Aikten (1983)

SUTL No.	Water Content (%)			Effective Dose Rate (mGy a^{-1})		
	Fractional	Saturated	Assumed	Beta[a]	Gamma	Total[b]
2382	12.5	21.6	16 ± 5	0.61 ± 0.05	0.40 ± 0.06	1.01 ± 0.08
2383	11.6	19.8	15 ± 4	0.61 ± 0.05	0.37 ± 0.05	0.98 ± 0.08
2384	7.8	21.6	15 ± 7	0.53 ± 0.05	0.33 ± 0.05	0.86 ± 0.07

Table D-3: Water contents, and effective beta and gamma dose rates following water correction.

[a] Effective beta dose rate combining water content corrections with inverse grain size attenuation factors obtained by weighting the 200 μm attenuation factors of Mejdahl (1979) for K, U, and Th by the relative beta dose contributions for each source determined by Gamma Spectrometry.

[b]Including a cosmic ray dose-rate contribution – 0.185 ± 0.05 – based on Prescott and Hutton (1994)

E. Quartz SAR OSL Measurements

E.1 Sample preparation

All sample handling and preparation was conducted under safelight conditions in the SUERC luminescence dating laboratories. Approximately 10-15 g of material from the core of the sample was processed for luminescence measurements, to separate sand-sized quartz and feldspar grains from the bulk sediment. The sample was wet sieved to obtain the 90-150 and 150-250 μm fractions. The 150-250 μm sub-sample was treated with 1 M hydrochloric acid (HCl) for 10 minutes, 15% hydrofluoric acid (HF) for 15 minutes, and 1 M HCl for a further 10 minutes. This etched material was then centrifuged in sodium polytungstate solutions of ~2.51, 2.58, 2.62, and 2.74 gcm^{-3}, to obtain concentrates of alkali feldspar (2.51-2.58 gcm^{-3}), plagioclase feldspar (2.58-2.62 gcm-3) and quartz (2.62-2.74 gcm^{-3}). The selected quartz fraction was then subjected to further HF and HCl washes (40% HF for 40mins, followed by 1M HCl for 10 mins). All materials were dried at 50°C and transferred to Eppendorf tubes. Purity of quartz fractions was then checked using scanning electron

microscopy. It was noted that a few percent of quartz grains, not restricted to any individual sample, contained feldspar micro-inclusions. The 150-250 μm quartz fractions were dispensed onto the central part of 1 cm diameter, 0.25 mm thick stainless steel disks, using silicone oil for adhesion.

E.2 Analytical procedure

SAR OSL measurements were conducted using the Risø DA-15 automatic reader (Bøtter-Jensen et al., 2000). The discs of quartz grains from the tube samples were subjected to a single aliquot regeneration (SAR) sequence (cf. Murray and Wintle, 2000). According to this procedure, the OSL signal level from an individual disc is calibrated to provide an absorbed dose estimate (the equivalent dose) using an interpolated dose-response curve, constructed by regenerating OSL signals by beta irradiation in the laboratory. Sensitivity changes which may occur as a result of readout, irradiation and preheating (to remove unstable radiation-induced signals) are monitored using small test doses after each regenerative dose. Each measurement is standardised to the test dose response determined immediately after its readout, to compensate for observed changes in sensitivity during the laboratory measurement sequence. For the purposes of interpolation, the regenerative doses are chosen to encompass the likely value of the equivalent (natural) dose. A repeat dose point is included to check the ability of the SAR procedure to correct for laboratory-induced sensitivity changes (the "recycling test"; 1 Gy; Table E-1), a zero dose point is included late in the sequence to check for thermally induced charge transfer during the irradiation and preheating cycle (the "zero cycle"; Table E-1), and an IR response check is included to assess the magnitude of non-quartz signals (1 Gy; Table E-1). Regenerative dose response curves were constructed using doses of 1, 5, 10 and 30 Gy, with a test dose of 2 Gy (Table E-1). In the present study, 16 discs per sample were measured using 4 discs each at 4 different preheats (Table E-1).

Aliquot	Operation	Cycle:	1	2	3	4	5	8	9	10
		Details	Natural					Zero	Recycling	IR Response
1-20	Regenerative Dose	"X" Gy $^{90}Sr/^{90}Y$	no	1	5	10	30	0	1	1
1-5	Preheat	200°C for 30s	yes	yes	yes	yes	yes	yes	yes	yes
6-10	Preheat	220°C for 30s	yes	yes	yes	yes	yes	yes	yes	yes
11-15	Preheat	240°C for 30s	yes	yes	yes	yes	yes	yes	yes	yes
16-20	Preheat	260°C for 30s	yes	yes	yes	yes	yes	yes	yes	yes
1-20	Measurement	IRSL 60s at 50°C	no	no	no	no	no	no	no	yes
1-20	Measurement	OSL 60s at 125°C	yes	yes	yes	yes	yes	yes	yes	yes
1-20	Test Dose (Td)	"X" Gy $^{90}Sr/^{90}Y$	2	2	2	2	2	2	2	2
1-5	Td Preheat	200°C for 30s	yes	yes	yes	yes	yes	yes	yes	yes
6-10	Td Preheat	220°C for 30s	yes	yes	yes	yes	yes	yes	yes	yes
11-15	Td Preheat	240°C for 30s	yes	yes	yes	yes	yes	yes	yes	yes
16-20	Td Preheat	260°C for 30s	yes	yes	yes	yes	yes	yes	yes	yes
1-20	Test Measurement	OSL 60s at 125°C	yes	yes	yes	yes	yes	yes	yes	yes

Table E-1: Quartz Single Aliquot Regenerative (SAR) Sequence

E.3 Single aliquot equivalent dose determinations

For equivalent dose determination, data from single aliquot regenerative dose measurements were analysed using the Risø TL/OSL Viewer programme to export integrated summary files that were analysed in MS Excel and SigmaPlot. Composite dose response curves were constructed from selected discs and for each of the four preheating groups from each sample, and used to estimate equivalent dose values for each individual disc and their combined sets. Dose response curves for each of the preheating temperature groups and the combined data were determined using a fit to an exponential function (Fig. E-1). The equivalent dose was then determined for each aliquot using the corresponding exponential fit parameters.

The distribution in equivalent dose values was examined using radial plotting methods and weighted mean histogram plots. Single aliquots were rejected from further analysis based on the sensitivity check, robust statistics, feldspar contamination and radial plots. Table E-2 summarises the quality evaluation checks on the SAR data (once filtered); the mean sensitivity of each aliquot and sensitivity change, the recycling ratio and zero dose response.

F. Age calculations

The total dose rate is determined from the sum of the equivalent beta and gamma dose rates, and the cosmic dose rate. Age estimates are determined by dividing the equivalent stored dose by the dose rate. Uncertainty on the age estimates is given by combination of the uncertainty on the dose rates and stored doses, with an additional 5% external error. Table F-1 lists the total dose rate, stored dose and corresponding age of the sample.

The dates are discussed in the main body of the report.

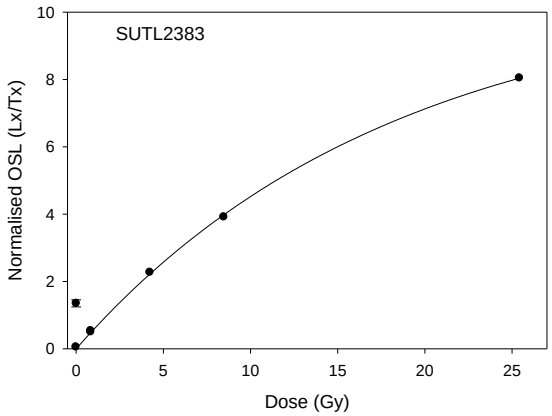

Figure E-1: Composite dose response curves for samples SUTL2383 to 2384.
For all samples - Lx = 1, 5, 10, 30 and 1 Gy; Tx = 2Gy

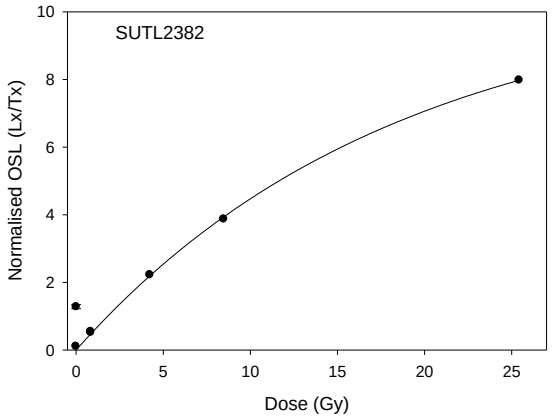

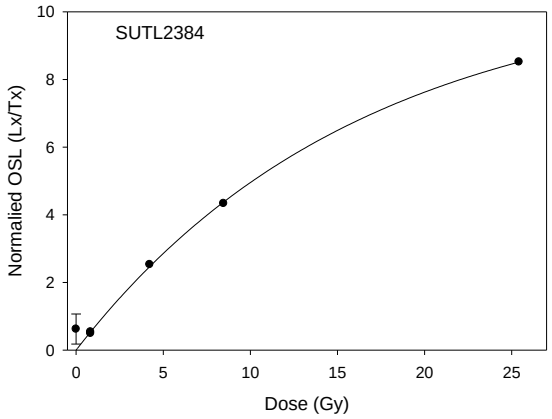

SUTL No.	Mass (mg)	Sensitivity (counts/Gy)	Sensitivity change (%)	Recycling Ratio	Zero Dose (Gy)	IR Response
2382	1.00	11289 ± 57	5.05 ± 1.85	0.98 ± 0.01	0.08 ± 0.02	0.18 ± 0.33
2383	0.97	6667 ± 46	5.13 ± 2.49	0.95 ± 0.02	0.06 ± 0.01	-0.8 ± 0.32
2384	1.00	3024 ± 26	6.94 ± 5.17	0.93 ± 0.06	0.57 ± 0.38	1.4 ± 3.54

Table E-2: SAR quality parameters

SUTL No.	Field No.	Location	Dose Rate (mGy a^{-1})	Stored Dose (Gy)	Age (ka)	Calendar years
2382	D04	Dhiarzos	1.01 ± 0.08	2.23 ± 0.02	2.20 ± 0.17	-189.7 ± 168.8
2383	D02	Dhiarzos	0.98 ± 0.08	2.32 ± 0.02	2.36 ± 0.18	-354.9 ± 183.7
2384	D01	Dhiarzos	0.86 ± 0.07	0.40 ± 0.09	0.46 ± 0.11	1549.8 ± 109.6

Table F-1: Total dose rates, stored dose and age estimates

Appendix B: Fault trends in the bedrock geology

Co-ordinates						Fault/Fracture Plane					Lineation			
Latitude			Longnitude			Plane measured	Displacement	Strike	Dip	Dip Direction	Lineation measured	Plunge	Trend	Sense
N	34	43.736	E	32	35.533	fracture		142	sub-vertical					
N	34	43.736	E	32	35.533	fracture		163	sub-vertical					
N	34	43.736	E	32	35.533	fracture		70	sub-vertical					
N	34	43.736	E	32	35.533	fracture		168	sub-vertical					
N	34	43.736	E	32	35.533	fracture		160	sub-vertical					
N	34	43.736	E	32	35.533	fracture		78	sub-vertical					
N	34	43.736	E	32	35.533	fault	cm-scale	145	43	SW				
N	34	43.736	E	32	35.533	fault	cm-scale	148	60	SW				
N	34	43.736	E	32	35.533	fault	cm-scale	170	60	W	slickenline	60	222	normal
N	34	43.736	E	32	35.533	fault	cm-scale	178	60	W				
N	34	43.687	E 32	36	35.646	fault	m-scale	172	70	W	slickenline	70	270	reverse
N	34	43.687	E 32	36	35.646	fault	m-scale	178	78	W	slickenline	64	238	?
N	34	43.687	E 32	36	35.646	fault	m-scale	174	68	W				
N	34	43.687	E 32	36	35.646	fault	m-scale	170	68	W	slickenline	68	254	normal
N	34	43.687	E 32	36	35.646	fault	cm-scale	178	50	E				
N	34	43.687	E 32	36	35.646	fault	cm-scale	2	58	E	slickenline	40	68	normal
N	34	43.687	E 32	36	35.646	fault	cm-scale	14	40	E	slickenline	20	74	?
N	34	43.687	E 32	36	35.646	fault	m-scale	160	48	W				
N	34	43.687	E 32	36	35.646	fault	m-scale	168	64	W	slickenline	64	252	normal
N	34	43.687	E 32	36	35.646	fault	m-scale	160	74	W	slickenline	74	252	normal
N	34	43.687	E 32	36	35.646	fault	m-scale	158	48	NE				
N	34	43.687	E 32	36	35.646	fault	m-scale	172	68	E				
N	34	43.687	E 32	36	35.646	fault	cm-scale	160	62	E	slickenline	62	22	?
N	34	43.687	E 32	36	35.646	fault	cm-scale	174	72	E				
N	34	43.669	E	32	35.684	fracture		84	74	N				
N	34	43.669	E	32	35.684	fracture		162	52	W				
N	34	43.669	E	32	35.684	fault	m-scale	158	74	NE	slickenline	70	78	?
N	34	43.669	E	32	35.684	fault	m-scale	164	54	E	slickenline	54	74	normal
N	34	43.669	E	32	35.684	fault	m-scale	154	84	NE	slickenline	80	60	normal
N	34	43.669	E	32	35.684	fault	m-scale	170	74	E	slickenline	74	58	normal

Appendix C: Clast assemblages in sediment associated with the various regional erosion surfaces

Coordinates		Location	Geology	Grain size	Clast type										
Latitude	Longnitude				Chalk	Grey chert	Bioclastic limestone	Calcarenite - Medium-grained	Calcarenite - Coarse-grained	Red mudstone	Red chert	Basalt	Dolerite	Coarse crystalline diorite	Gabbro	Ultramafics
N3443.639	E3235.727	Intersection of Sousikou-Laona access road with Vathyrkakas ravine	F2? channelised conglomerate	> 5cm in Ø	31		1	20	3							
N3443.639	E3235.727	Intersection of Sousikou-Laona access road with Vathyrkakas ravine	F2? channelised conglomerate	< 5cm in Ø	36	1		6		2	3		9			2
N3443.683	E3235.648	Intersection of Sousikou-Laona access road with Vathyrkakas ravine	F2? channelised conglomerate	> 5cm in Ø	18	4		29					1			
N3443.683	E3235.648	Intersection of Sousikou-Laona access road with Vathyrkakas ravine	F2? channelised conglomerate	< 5cm in Ø	26						1	1	8			
N3443.665	E3235.649	Most recent fill of the Vathyrkakas stream	Recent' fill of the Vathyrkakas ravine	> 5cm in Ø	21		2	13					2			
N3443.665	E3235.649	Most recent fill of the Vathyrkakas stream	Recent' fill of the Vathyrkakas ravine	< 5cm in Ø	17		1	7			1		1			
N3443.412	E3236.415	Roadcut on on the Kouklia-Archimandrita road	F0? Marine conglomerates	> 5cm in Ø	6	2	10				1	5	13		1	3
N3443.412	E3236.415	Roadcut on on the Kouklia-Archimandrita road	F0? Marine conglomerates	< 5cm in Ø	4		3		2	1	2	3	12		1	1
N3442.678	E3224.762	Roadcut on on the Kouklia-Archimandrita road, by Kouklia	F1/2 Fanglomerate	> 5cm in Ø												
N3442.678	E3224.762	Roadcut on on the Kouklia-Archimandrita road, by Kouklia	F1/2 Fanglomerate	< 5cm in Ø	19						7		134		16	4
N3443.095	E3234.622	Roadcut on the Kouklia-Nikokleia road	F2? channelised conglomerate	< 5cm in Ø	5	2	6						29		4	
N3443.436	E3234.703	Mouth of Vathyrkakas Ravine	F3? channelised conglomerate	< 5cm in Ø	18		4	24					5			
N3443.095	E3234.622	Probable F2 channel fill	F2 channelised conglomerate		11			3			2		37	28	25	
N3443.436	E3234.703	Dhiarzos river bed	Recent' fill of the Dhiarzos River		26		33	7			3		32	7	10	